Talanta 128 (2014) 132–140

Contents lists available at ScienceDirect

Talanta

journal homepage: www.elsevier.com/locate/talanta

Lead detection using micro/nanocrystalline boron-doped diamond by square-wave anodic stripping voltammetry

Tatiane M. Arantes [a,*], André Sardinha [b], Mauricio R. Baldan [a], Fernando H. Cristovan [b], Neidenei G. Ferreira [a]

[a] LAS/INPE-Instituto Nacional de Pesquisas Espaciais, Av. dos Astronautas 1758, São José dos Campos-SP, Brazil
[b] Universidade Federal de São Paulo, Instituto de Ciência e Tecnologia, R. Talin 330, José dos Campos-SP, Brazil

ARTICLE INFO

Article history:
Received 13 January 2014
Received in revised form
24 April 2014
Accepted 25 April 2014
Available online 6 May 2014

Keywords:
Boron-doped diamond
Nanocrystalline diamond
Lead
Heavy metals
Square-wave voltammetry

ABSTRACT

Monitoring heavy metal ion levels in water is essential for human health and safety. Electroanalytical techniques have presented important features to detect toxic trace heavy metals in the environment due to their high sensitivity associated with their easy operational procedures. Square-wave voltammetry is a powerful electrochemical technique that may be applied to both electrokinetic and analytical measurements, and the analysis of the characteristic parameters of this technique also enables the mechanism and kinetic evaluation of the electrochemical process under study. In this work, we present a complete optimized study on the heavy metal detection using diamond electrodes. It was analyzed the influence of the morphology characteristics as well as the doping level on micro/nanocrystalline boron-doped diamond films by means of square-wave anodic stripping voltammetry (SWASV) technique. The SWASV parameters were optimized for all films, considering that their kinetic response is dependent on the morphology and/or doping level. The films presented reversible results for the Lead [Pb (II)] system studied. The Pb (II) analysis was performed in ammonium acetate buffer at pH 4.5, varying the lead concentration in the range from 1 to 10 $\mu g\ L^{-1}$. The analytical responses were obtained for the four electrodes. However, the best low limit detection and reproducibility was found for boron doped nanocrystalline diamond electrodes (BDND) doped with 2000 $mg\ L^{-1}$ in B/C ratio.

1. Introduction

The trace detection of toxic or heavy metal ions in water is essential for the human health and environmental safety. There are numerous health problems caused by the exposure of humans with high levels of heavy metal ions (Cd^{2+}, Pb^{2+}, Hg^{2+}, $As^{3+/5+}$). Moreover, these toxic ions tend to accumulate in the body with a slow removal rate. For example, the biological half-life of cadmium is from 10 to 30 years, while the presence of lead in the bone is more than 20 years [1]. The Environmental Protection Agency (EPA) estimates that about 20% of human exposure to lead occurs through contaminated drinking water [1]. The monitoring of these contaminants with adequate selectivity, sensitivity and reproducibility is essential for the government rules impose the maximum permissible exposure levels of these heavy metals in the water to protect public health. The monitoring process is available using various techniques, such as: atomic absorption, atomic emission, and electrochemical techniques [1]. Alternatively, electroanalytical techniques have attractive features, including sensitivity, easy operational procedures, and portability. However, the conventional electroanalytical determination of metals typically involves the use of mercury-based electrodes, for example, hanging mercury drop electrode (HMDE) [2,3] or electrodes coated with mercury, and glassy carbon [1,4] or iridium [5,6] substrates. The mercury electrode is considered standard for analysis of dissolved metals. However, mercury toxicity has been a great concern of environmentalists and it has motivated several researches for the development of mercury-free electrodes [1,5].

Boron doped diamond (BDD) electrodes have been extensively studied due to their attractive electrochemical properties, mainly including: high thermal conductivity; high hardness and chemical inertness; a wide electrochemical potential window in aqueous and non-aqueous media; a very low capacitance and a very high electrochemical stability [1,2,7]. These properties have favored the use of diamond to detect a variety of analytes, including traces of heavy metals as well as pesticide determinations, substituting the mercury electrodes in analytical techniques [8–11]. Taking into account the boron-doped diamond films, the production of nanocrystalline diamond films (BDND) may result in the increase of

* Corresponding author at: LAS / INPE - National Institute for Space Research, Av. dos Astronautas, 1758, Jd. da Granja, 12227-010 Sao Jose dos Campos – SP, Brazil. Tel.: +55 12 208 6675; fax: +55 12 3308 6717.
E-mail address: tmarantes@yahoo.com.br (T.M. Arantes).

http://dx.doi.org/10.1016/j.talanta.2014.04.074
0039-9140/

electroactive area due to the reduction of diamond grain size, promoting their improving of analytical sensibility and selectivity [1,12,13]. Considering the electrochemical characteristics of sensors based on boron-doped nanocrystalline diamond (BDND), several studies have reported promising results for these electrodes as fast response, low detection limit, high stability, and excellent response accuracy [14–17]. In addition, nanocrystalline films provide a better catalytic activity, decreasing the overpotential of certain oxidation–reduction reactions [18].

Some studies found in the literature have demonstrated the importance of boron-doped nanocrystalline diamond electrodes. May et al. [19] have studied the relationship between the film morphology, conductivity and boron doping level. They suggested that the production of electrodes with controlled roughness and conductivity can be considered excellent candidates for electrochemical applications. Sonthalia et al. [20] made a comparison between the boron-doped nanodiamond electrodes with mercury electrodes for the detection and quantification of Ag (I), Cu (II), Pb (II), Cd (II) and Zn (II) in several water samples. They concluded that the diamond electrode has the same properties from those of mercury, but without toxicity in addition to its chemical inertia and non-volatility. Recently, Honório et al. [21] used nanocrystalline boron-doped diamond electrode for the determination of Cu(II), Pb(II), Cd (II) and Zn(II) in honey by differential pulse anodic stripping voltammetry (DPASV) and showed detection limits of 0.37, 0.40, 1.28 and 0.16 mg L^{-1} were found for Cu, Pb, Cd and Zn, respectively.

Many electroanalytical methods employ the adsorptive accumulation in the HMDE combined with different stripping voltammetric techniques. One of the most sensitive techniques is the square-wave voltammetry [22,23]. Square-wave voltammetry (SWV) is a powerful electrochemical technique applied in both electrokinetic and analytical measurements. The detection limits can be compared with the chromatographic and spectroscopic techniques [24–27]. Furthermore, the analysis of the characteristic parameters of this technique enables to estimate the mechanism and kinetic of the electrochemical processes in study. Thus, SWV allows analyzing the reversible, irreversible and quasi-reversible electrode reactions, considering the correlations between the following parameters: frequency, period, square-wave potential, and amplitude [21,26,28].

In this work, four types of diamond electrodes of BDD, BDND, and BDUND were produced and characterized in addition to their application to lead detection in ultra pure synthetic electrolytes, using square wave anodic stripping voltammetry (SWASV) technique. For this purpose, a systematic study was conducted using theoretical models of SWV [20–24,29,36,37] to investigate the mechanisms and kinetics for these different diamond electrodes, considering the Pb (II) system as a function of their doping level and grain size. The voltammetric parameters were optimized for all electrodes, taking into account the following results: (1) SWV curves for the net current (I); its forward (I_f) and backward (I_b) components; (2) the dependence of the net peak current of reversible reaction as a function of the frequency square-root; (3) the dependence of the net peak current (I) and net peak current /peak current width at half-height ratio ($I/\Delta E_{p/2}$) as a function of the square wave amplitude (E_{SW}); and (4) the dependence of the net peak current (I) as a function of the step potential (ΔE_s). Afterwards, these parameter optimizations for Pb (II) system and the analytical curves were obtained in pure electrolyte by the standard addition method.

2. Experimental

Four different types of diamond films were produced in a hot filament chemical vapor deposition (CVD) reactor with two different boron doping levels in silicon substrates. Boron was obtained from an additional H_2 line passing through a bubbler containing trimethyl borate (Aldrich, 99%) dissolved in methanol with dissolution of 2000 or 20,000 mg L^{-1}. BDD films were grown at 800 °C for 16 h at 40 Torr with a gas mixture of 1.5% CH_4 and 98.5% H_2. BDND_2000 and BDND_20,000 films were obtained at 650 °C for 16 h at constant pressure of 30 Torr and gas mixture of 1.5% CH_4, 80% Ar and 18.5% H_2. The morphologies of the films were observed by scanning electron microscopy (SEM) using a JEOL JSM-5310 model. Diamond film quality were verified by micro-Raman scattering spectroscopy (Renishaw microscope system 2000) using the 514.5 nm line of an argon ion laser, taking the spectra covering in the range from 300 to 3500 cm^{-1}. The crystallinity and the grain size of the films were investigated by XRD using a high resolution Philips diffractometer, X'Pert model, with CuK_α radiation ($\lambda = 1.54$ Å) in grazing incidence mode, incident angle of 2° and resolution limit of 0.02° for all samples.

The electrochemical measurements were made using an Autolab PGSTAT 302 equipment with a three-electrode cell. The BDD or BDND films obtained with two B/C ratios were used as working electrode. The geometric area of the BDD films in contact with the electrolyte was 0.23 cm^2. A platinum coil wire served as counter electrode and Ag/AgCl was used as reference electrode. The Mott–Schottky plots (MSP) measurements were performed for each sample at single sine wave potential of 10 mV peak-to-peak potential perturbations. The MSP curves were taken in 0.5 mol L^{-1} H_2SO_4 solution at three different frequencies (1, 10 and 50 kHz).

The square wave anodic stripping voltammetry (SWASV) experiments were performed in the Pb (II) standard solution using 100 μg L^{-1} $Pb(NO_3)_2$ in 0.2 mol L^{-1} ammonium acetate buffer (pH 4.5) at pH 4.5, purging nitrogen for 5 min in the following different steps: (a) the pre-conditioning step, applying the potential of 0.9 V vs. Ag/AgCl for 45 s before each measurement in order to ensure the dissolution of the remaining deposits on the electrode surface, (b) the pre-concentration step procedure at −1.2 V vs. Ag/AgCl for 180 s, the solution was stirred during the electrodeposition step and (c) the SWASV voltammograms recorded from −0.8 V to 0.0 V. For the optimization of SWASV parameters, the Lead concentration was 100 μg L^{-1}.

After optimization of the voltammetric parameters, analytical curves were obtained in pure electrolyte by the standard addition method in the lead concentration in the range from 1 to 10 μg L^{-1}. In order to estimate the detection and quantification limits (DL and QL), three blank voltammograms were measured in purified electrolyte at oxidation potential of Pb (II). The standard deviation (S_b) was obtained by the average current of these voltammograms. The slope of the straight line (b) was obtained from the analytical curves ($DL = 3S_b/b$ and $QL = 10S_b/b$) [22,23].

3. Results and discussions

3.1. Diamond characterization

The morphology and structure of these films showed different properties. The SEM images allowed observing the morphology of diamond films, as shown in Fig. 1. Significant changes in the diamond grain sizes were observed due to the doping level and addition of argon to the gas mixture. For BDD films (Fig. 1a and b), the decreasing in the diamond grain size is expected when is increased the boron incorporation, causing a reduction in the growth rate [25]. According to Issaoui et al. [30] boron affects the nucleus formation during the first step of growth. Consequently, high doping levels promote a low growth rate compared with the values obtained using low doping levels. However, the change in growth rate cannot be related only to the influence of boron. A small amount of oxygen from the solution can also contribute to

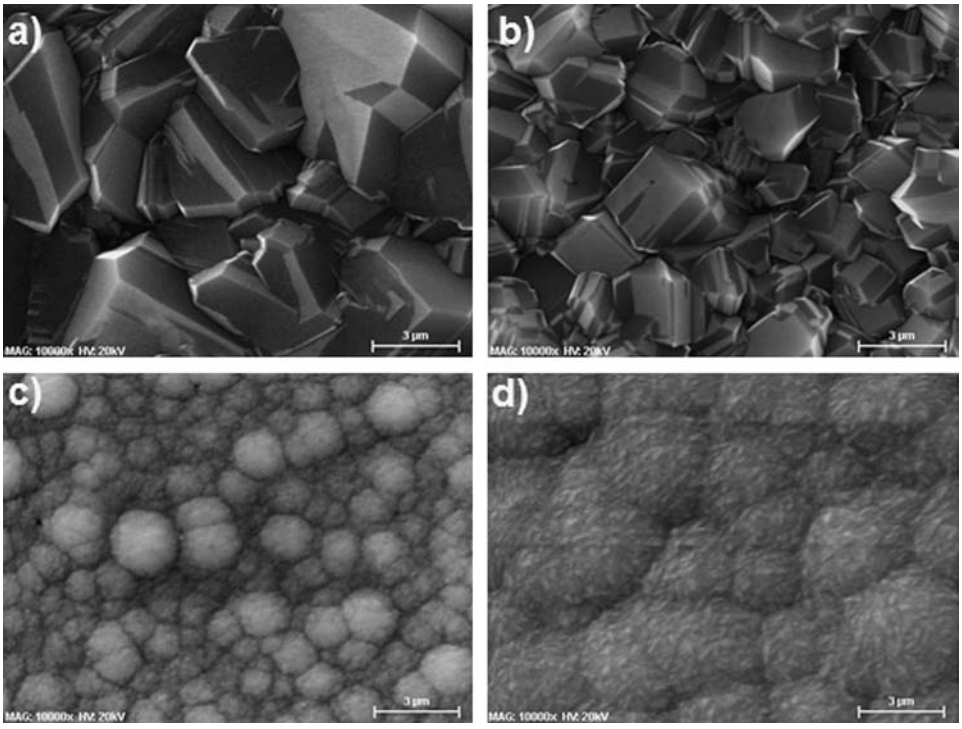

Fig. 1. SEM images of diamond films: (a) BDD 2000, (b) BDD 20,000, (c) BDND 2000 and (d) BDND 20,000.

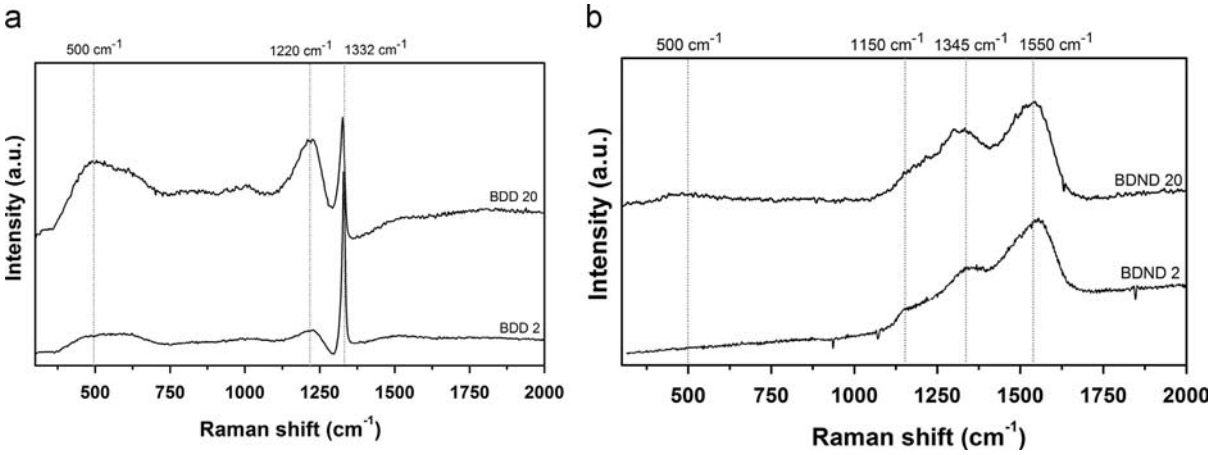

Fig. 2. Raman spectra of (a) BDD 20,000 and BDD 2000 and (b) BDND films with 80% Ar with 20,000 and 2000 ppm B/C ratio.

the growth rate variation. Oxygen is known to lead to potential chemical reactions with species in the gas phase and to the consumption of some carbon and boron species in the plasma, which usually reduces the diamond growth rate. The films grown without argon, and with 2000 and 20,000 mg L^{-1} in B/C ratio presented an uniform morphology with well-faceted microcrystalline surface and grain sizes at around 3.0 and 1.5 μm, respectively. Furthermore, for the BDND films grown with 80% of argon, in both doping levels there is a surface with small grains which tend to form small agglomerates, suggesting a secondary nucleation or re-nucleation process [26]. In relation to the BDND growth process, its non-columnar characteristics reflect in a low surface roughness formed by grain clusters. The addition of argon caused the lower dissociation of molecular hydrogen on the filament, decreasing the amount of atomic hydrogen that reaches the substrate and, consequently, reducing the diamond grain size [31–33].

According to the Raman spectra (Fig. 2), the films grown without the presence of argon showed a clear and intense diamond peak at 1332 cm^{-1}, which is characteristic of microcrystalline films [34]. Nevertheless, for the films grown with 80% of argon, the diamond peak is overlapped by the *D* band (1345 cm^{-1}). This behavior is commonly observed in visible Raman spectra of nanocrystalline diamond films [26,28]. The bands located at 1150 and 1490 cm^{-1}, which are arising from the transpolyacetylene (TPA) present in the grain boundaries, were identified only in samples with high argon concentration (80%) [35,36]. For the BDND films, the graphite G band at around 1550 cm^{-1} indicates a high presence of sp^2 carbon. The bands at 500 and 1220 cm^{-1}, related to the boron doping, were found in all spectra and they are more evident for the BDD films. These bands are still subject of debate and they are commonly associated with the real incorporation of boron into the diamond lattice [18,37]. The presence of the band at 500 cm^{-1} is attributed to the local vibration modes caused by the increase of boron concentration [38]. In addition, the broad band centered at 1230 cm^{-1} is associated to the Fano effect interference between the discrete phonon state and electronic continuum. This effect is ascribed to

the transition from the broadened impurity band to continuum states composed of excited acceptor and valence band states [12]. Comparing the BDD and BDND films in the same doping level, the bands at 500 and 1220 cm^{-1} in the Raman spectra are less evident for the films grown with the presence of Ar. This behavior may be associated with the increase of boron incorporation in the diamond grain boundaries for BDND films because of their high sp^2 content. May et al. [18] used Raman spectroscopy to detect substitutional boron in nanodiamond films, and estimated that 80% of the boron incorporated into the BDND was found in the surface region of the grains and sp^2 bonds in the grain boundaries. They concluded that the band at 1220 cm^{-1} is less prominent for nanodiamond films that present cauliflower-like morphology, than those with faceted morphology. This behavior was clearly observed in our films, as it can be seen in Fig. 2. Ferrari et al. [39] showed that this band disappear when the morphology changes from micro to nanocrystalline. The reason is that the majority of the *B* is present at sites that do not contribute for the continuum electronic states. These sites include interstitials, crystallite surfaces, or nondiamond carbon impurities verified in the grain boundaries.

The XRD patterns of all films are shown in Fig. 3, where the diamond diffraction peaks at around 44°, 75°, and 91° correspond to the (111), (220), and (311) crystallographic planes, respectively, confirming the existence of crystalline diamond [25]. On the other hand, the high intensity of the (111) peak in these films has been reported as a sign of the existence of a high quality diamond phase [23]. A competitive effect between the different planes occurs during the growth of polycrystalline film, i.e., some crystalline orientations grow faster than others. As the film becomes thicker, some orientations overlap the others [25,26]. For the CVD diamond, it is well established that the growth rate of the (111) planes is higher than those in the (110) and (100) planes [25]. For the BDNC films, which showed an absence of well-faceted crystals, it is reasonable to assume that the nanometric (110) growth sectors develop faster than the others, resulting in structures elongated along the (110) axis. Silva et al. [40] have proposed a mechanism where the first growth sectors develop randomly around the seed grains and some of them could have their fastest growth direction assumed to be the (110) axis. The full width at half maximum (FWHM) of the (111) peak decreased with the increase of doping level for the BDD films. The FWHM of the BDND films increased with the doping level. This behavior can be explained due to the presence of both argon and boron, which influences in the growth of grains. The films with higher doping, BDND characteristic, exhibited a broader line width due to a smaller grain size and a higher sp^2 fraction of grain boundary. Particularly, for the BDND

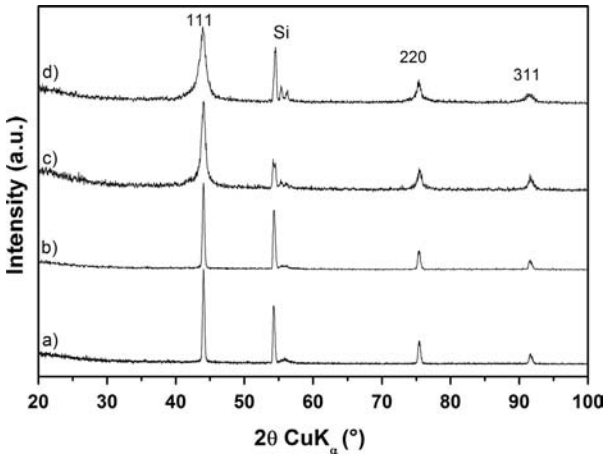

Fig. 3. XRD of diamond films: (a) BDD 20,000, (b) BDD 2000 (c) BDND 20,000 and (d) BDND 2000.

films, some authors have used the Scherrer's equation to estimate the crystal size from the most intense diffraction peak, i.e., (111) plane [25,34]. The crystal size (L) calculated vs. the doping level decreased from 11 to 7 nm when the doping level increased from 2000 to 20,000 mg L^{-1} B/C. It is important to point out that the crystallite size, calculated from the XRD broadening line of peaks may be strongly affected by the crystal defect density [28].

The measurements of differential capacitance in the space charge region for semiconductor/electrolyte interface can extend the understanding of the interfacial process. In addition, the number of acceptor densities can be calculated from the slope of the linear region of the Mott–Schottky plots (MSP) [41]. The results of acceptor concentrations using different values of frequency were very similar. The MSP analysis of the films showed an increase in the acceptor concentrations from 10^{19} to 10^{20} B cm^{-3} when the boron carbon/ratio increased from 2000 to 20,000 ppm for the BDD films. On the other hand, for the BDND films, the acceptor concentrations were approximately 10^{20} B cm^{-3} for both doping levels. The higher boron incorporation was verified for the BDND film of 2000 mg L^{-1} than those of BDD film of 2000 ppm, which can be associated with the reduction of grain size. The high density of diamond grains detected in the film BDND can be responsible for the higher acceptor values observed on the MSP measurements.

3.2. Parameters optimization for square wave anodic stripping voltammetry

The square wave voltammetry (SWV) has advantages of obtaining the peak current defined at high scan speeds with better sensitivity and reduced background noise compared to those of other voltammetric techniques. This sensitivity is associated with the applied pulse to generate the forward and backward currents, which causes a symmetrical peak current concerning its position, width, and intensity characteristic for each evaluated system [25,26,42]. Theoretical calculations were performed by Osteryoung [42] and Lovric [43] using simulation of reversible, irreversible and quasi-reversible reactions to explain the SWV measurements. These calculations showed that the voltammogram characteristics (I_p, E_p and $\Delta E_{p/2}$) are linearly depending on some parameters used in the SWV (ν, E_{sw} and ΔE_s) as well as the kind of redox system employed. In this sense, the optimization of the initial measure parameters, such as: frequency (ν), amplitude (E_{sw}), and step potential (ΔE_s) has significant importance for the understanding of the system in analysis. Therefore, the response evaluations, after setting the parameters involved in the technique, the data interpretation is able to define the kind of reaction involved in each system studied. Moreover, it is possible to obtain information on the mechanism and the kinetics involved in the electrodic process.

The voltammogram is characterized by the maximum net response, which is also called the net peak current, denoted as $I_p = I_f - I_b$. In this case, I_f is the forward current (oxidative) and the I_b is backward current (reductive). The increase in the SWV sensitivity depends on the reversibility of the redox process [22]. The corresponding staircase potential is the net peak potential. Other characteristics are the minimum of the reductive component, the maximum of the oxidative component and their potentials. The net peak potential and the peak potentials of both components are independent of the SWV frequency. This is one of various indications that the electrode reaction is electrochemically reversible within the range of applied frequencies [21–25]. Using the above considerations, the square wave anodic stripping voltammetry (SWASV) experiments were performed to confirm the Pb (II) redox process on BDD and BDND at two different doping levels. The solution used was 100 μg L^{-1} Pb (II) standard in 0.2 mol L^{-1} ammonium acetate buffer (pH 4.5) for the potential

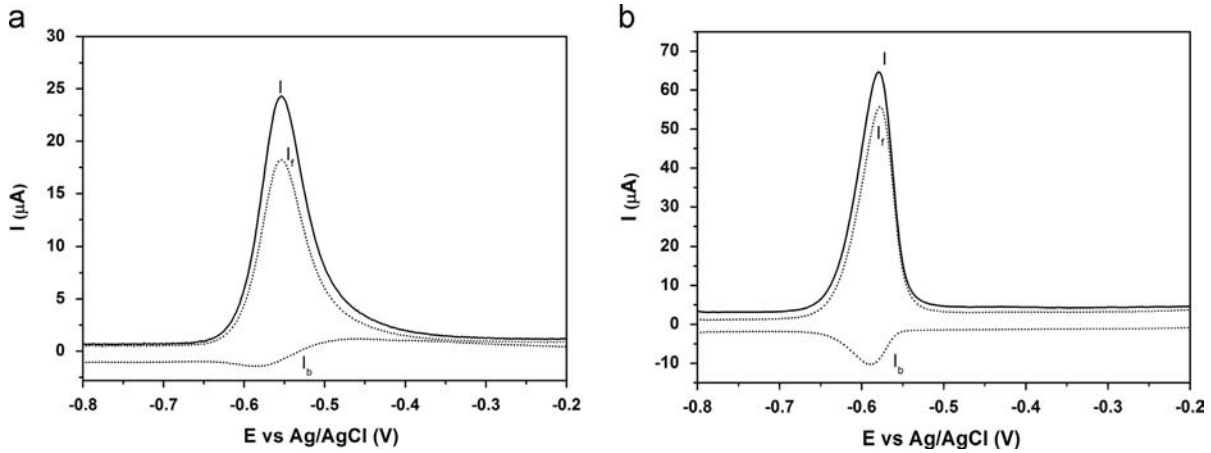

Fig. 4. SWASV for 100 μg/L Pb^{2+} in ammonium acetate buffer (0.2 mol L^{-1}), deposition time = 180 s, E_{sw} = 40 mV, ΔE_s = 2 mV and ν = 150 Hz. The net current (I) with its forward (I_f) and backward (I_b) components. (a) BDD 20,000 and (b) BDND 2000.

scan from −0.8 to 0.0 V, with ν = 150 Hz, E_{sw} = 50 mV and ΔE_s = 2 mV. For the four electrodes studied, one voltammetric peak towards the forward component and one peak towards the backward component of the currents were observed. A well-defined and symmetrical resultant curve was observed for all electrodes, as shown in Fig. 4, indicating that the voltammetric responses for the lead oxidation do not achieve the steady-state condition, as observed by Manivannan et al. [2] and McGaw et al. [7] using anodic stripping voltammetric analysis. The voltammograms in Fig. 4 showed that the contributions of the forward and backward currents for the net current are approximately equal and the difference between the two peak potentials (ΔE_p) is only 0.008 V. This behavior suggests that the oxidation of Pb to Pb (II) is reversible. The separation between E_p in forward and backward components for the Pb (II) was practically constant, with E_p values closer from those observed in resultant responses. In addition, the width at half-height ($\Delta E_{p/2}$) of the resultant peak and also the ratio between the forward and backward peaks decreased when ν values were increased. These responses are in agreement with the theoretical predictions for the SWV voltammograms in reversible redox reactions, which are affected by the surface electrode reactions with adsorbed reactants and products [22,41]. Some authors [22,23,39,43] consider the frequency used to apply the potential pulses is one of the most important variables in SWV because, keeping the concentration of the analyte constant, it is responsible for estimating the signal intensity, and consequently, the sensitivity obtained in the analysis.

The behavior of the peak current (I_p) as a function of the frequency variation applied to the potential pulses of ($1/\tau$) is related to the reversibility of the reaction. It is observed that for reversible systems, the increase in the current is proportional to square-root of frequency [24]

$$I_p = k_r \upsilon^{1/2} \quad (1)$$

where k_r is the reaction rate constant and ν is the frequency.

The increase of frequency in the applied potential pulses caused an increase in the current response, which improves the sensitivity analysis. However, this increase of frequency occurs by means of a reversible process and the peak current exponentially increases. Thus, this optimization must be considered in analytical curves. Fig. 5 shows that for all films, micro and nanocrystalline with 20,000 and 2000 mg L^{-1} B/C ratio, the relationship between the peak current and the square root of the frequency is linear. Consequently, these systems can be considered reversible in good agreement with Eq. (1). Considering initially the microcrystalline electrodes, both presented reversibility in the frequency range evaluated. Nevertheless, the electrode with higher doping (B/C: 20,000 mg L^{-1}) showed higher electrochemical sensitivity, considering the frequency variation due to its higher slope, as shown in Fig. 5(b). This behavior may be attributed to its higher doping level leading to its higher conductivity, as it was observed in the MSP measurements.

Fig. 6 shows the variation on the pulse amplitude at the peak current in the micro and nanocrystalline diamond films. The amplitude variation in the pulse potentials allows the evaluation of the kind of redox process. For the reversible reactions with adsorption of product and reactant, the peak current increases only in proportion to amplitude values less than 50 mV. The application of high pulse amplitude caused an increase in width half-heigth ($\Delta E_{p/2}$) of the peak current, influencing the voltammetric response. According to the theoretical models for the SWV [44], the increase in nE_{sw} promotes a continuous decreasing in the $\partial I/\partial nE_{sw}$ slope, while the $\partial \Delta E_{p/2}/\partial nE_{sw}$ gradient increases. The maximum ratio $I/\Delta E_{p/2}$ appears at around E_{sw} = 50 mV, as it can be seen in Fig. 6b and d. At higher amplitude values, the peak resolution decreased slightly [23]. This behavior agrees with the literature for the SWV [45–47] indicating that a higher heterogeneous electron transfer rate can be obtained. Similarly, several studies [48–51] for the polycrystalline diamond films have demonstrated that the heterogeneous electron-transfer reactions were considered because the physicochemical properties of sp^2 and sp^3 carbon electrodes influence their response, depending on the mechanistic aspects of the particular redox analyte.

The increase in step potential (ΔE_s) also improves the SWV analytical sensitivity as well as the increase of amplitude in the range from applied pulses. The effective variation in potential rate for the SWV is the product between the frequency and scan increment. Therefore, the last parameter also increases the signal and sensitivity of this technique. On the other hand, large ΔE_s values can promote a peak broadening, decreasing the measurement resolution. The influence of the step potential variation in net peak current is similar for the BDD films in both doping levels (Table 1) and the increase in ΔE_s not causes peak broadening. On the other hand, in both nanocrystalline films the step potential influences in the net peak current to the lead and the increase in ΔE_s promote a peak broadening. High ΔE_s values lead to a significant increase in the width of the peak current, resulting in a decreasing in the selectivity and sensitivity of SWV. One possible explanation for this behavior can be the difference in the reaction speed between one film and other. When the reaction speed is slow, the influence of ΔE_s is not observed, whereas for rapid reaction kinetics, there is a significant influence of ΔE_s in the lead

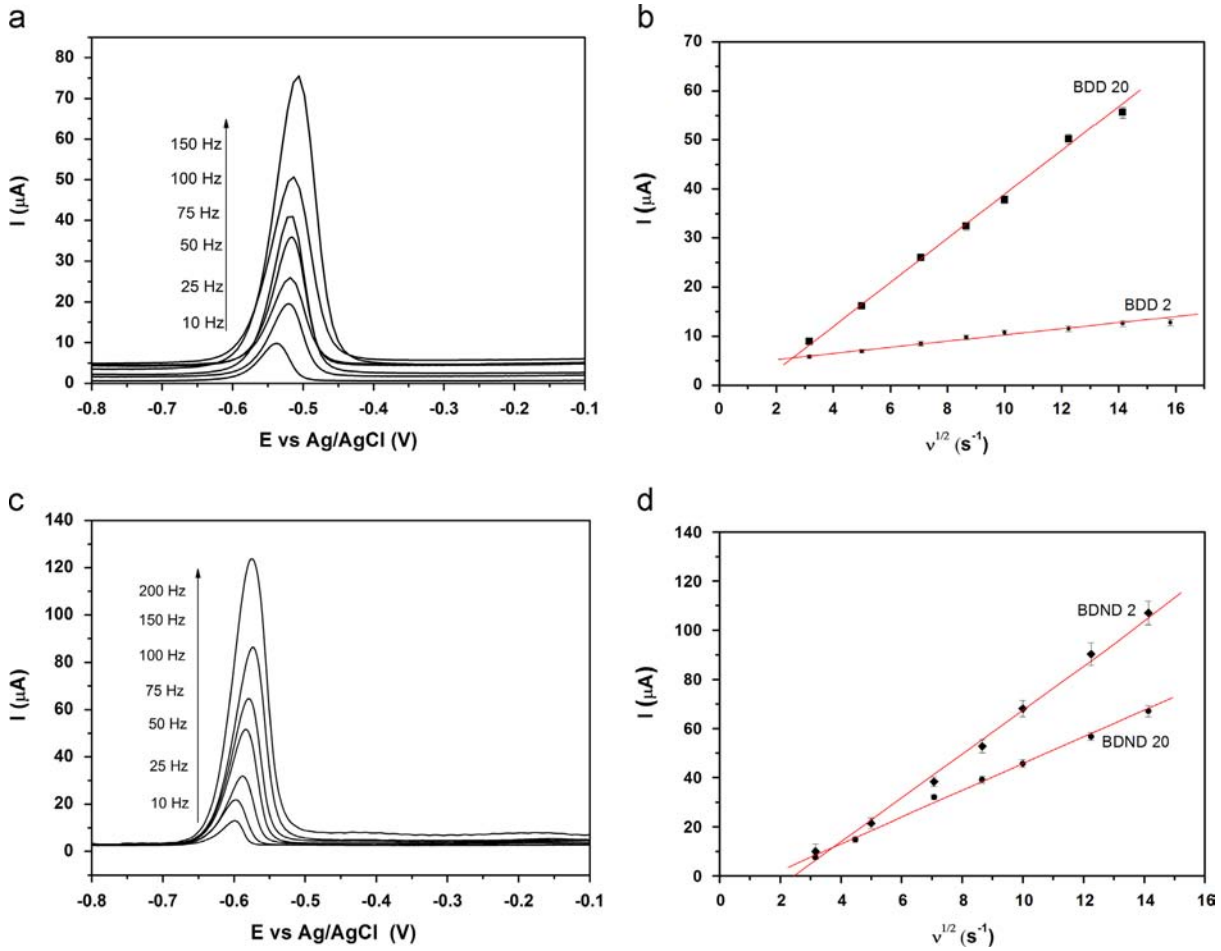

Fig. 5. SWASV curves as a function of the frequency for electrodes (a) and (b) microcrystalline films, (c) and (d) nanocrystalline, repectively. SWASV for 100 μg L^{-1} Pb^{2+} in a ammonium acetate buffer (0.2 mol L^{-1}), deposition time = 180 s, E_{sw} = 40 mV and ΔE_s = 2 mV.

electrochemical response. The peak potential constantly shifts towards more positive values when ΔE_s is increased. However, the peak current has a significant initial increment and then, a leveling when ΔE_s is greater than 4 mV. Therefore, a value of 2 mV was chosen for the analytical determinations in all films.

3.3. Lead detection

After the voltammetric parameter optimization for the SWV, analytical curves were obtained in pure electrolyte by the standard addition method using BDD and BDND films with both B/C ratios of 2000 or 20,000 ppm. Fig. 7a and c shows the SWASV stripping peaks for the Pb deposited from solutions with different Pb^{2+} concentrations from 0 to 10 μg L^{-1} in ammonium acetate buffer (pH 4.5), which presented a peak potential around −0.55 V vs. Ag/AgCl. The increase in the differential current as a function of the Pb concentration has practically a linear dependence. Fig.7b and d shows the analytical curve for the BDD 20,000 ppm and BDND 2000 ppm films, i.e, the linear dependence of I_p with Pb concentration for the studied interval (1–10 μg L^{-1}).

Thus, in this concentration range, the least-squares analysis yielded for the calibration graph merit figures [2,6,52], such as sensitivity, detection and quantification limits (DL and QL) which were calculated and listed in Table 2. DL is the lowest analyte concentration analysis that can be detected, but it can be not necessarily quantified by employing a given experimental procedure. QL is defined as the lowest analyte concentration that can be quantitatively determined. QL is the minimum concentration of detectable metal ion in each diamond film, as demonstrated in Table 2. The lead concentrations in the range from 1 to 10 μg L^{-1} were detectable using BDD and BDND, and showed similar values that the observed for the mercury electrodes and Hg-GC [2,7,47]. In addition, Table 2 shows the sensitivity, an important parameter in order to obtain the low detection limits. BDND exhibits a response sensitivity that is around five times greater than BDD for lead metal ions. Typically, a higher sensitivity result in a lower detection and quantification limits for which both nanodiamond films (BDND 2000 and 20,000 mg L^{-1} B/C ratio) is the minimum concentration detectable (μg L^{-1}). According to Dragoes et al. [47] in their study on the heavy metal detections with BDD films compared with mercury films in glass carbon (GC), while a direct comparison of the sensitivity is often useful for determining how well two electrodes perform analytically, it is not good to compare these two electrodes (diamond films and mercury electrodes). The metal phase formation on diamond is a 3-D process that depends on the surface area, whereas the formation of metal phase with Hg depends on its available volume. The relatively large volume of Hg formed on GC during the preconcentration step causes a higher sensitivity; however, because of the higher noise/background current, the Hg-CG values are comparable or inferior to BDD. Another work related to the detection of heavy metals using diamond electrodes was to McGaw et al. [7]. They used BDD for the anodic stripping voltammetric (ASV) determination of heavy metal ions such as, Cd (II), Pb (II) and Zn (II) and showed the linear dynamic range for BDD was three to four orders of magnitude ($r^2 > 0.995$), similar to Hg-GC, but the sensitivity for BDD was

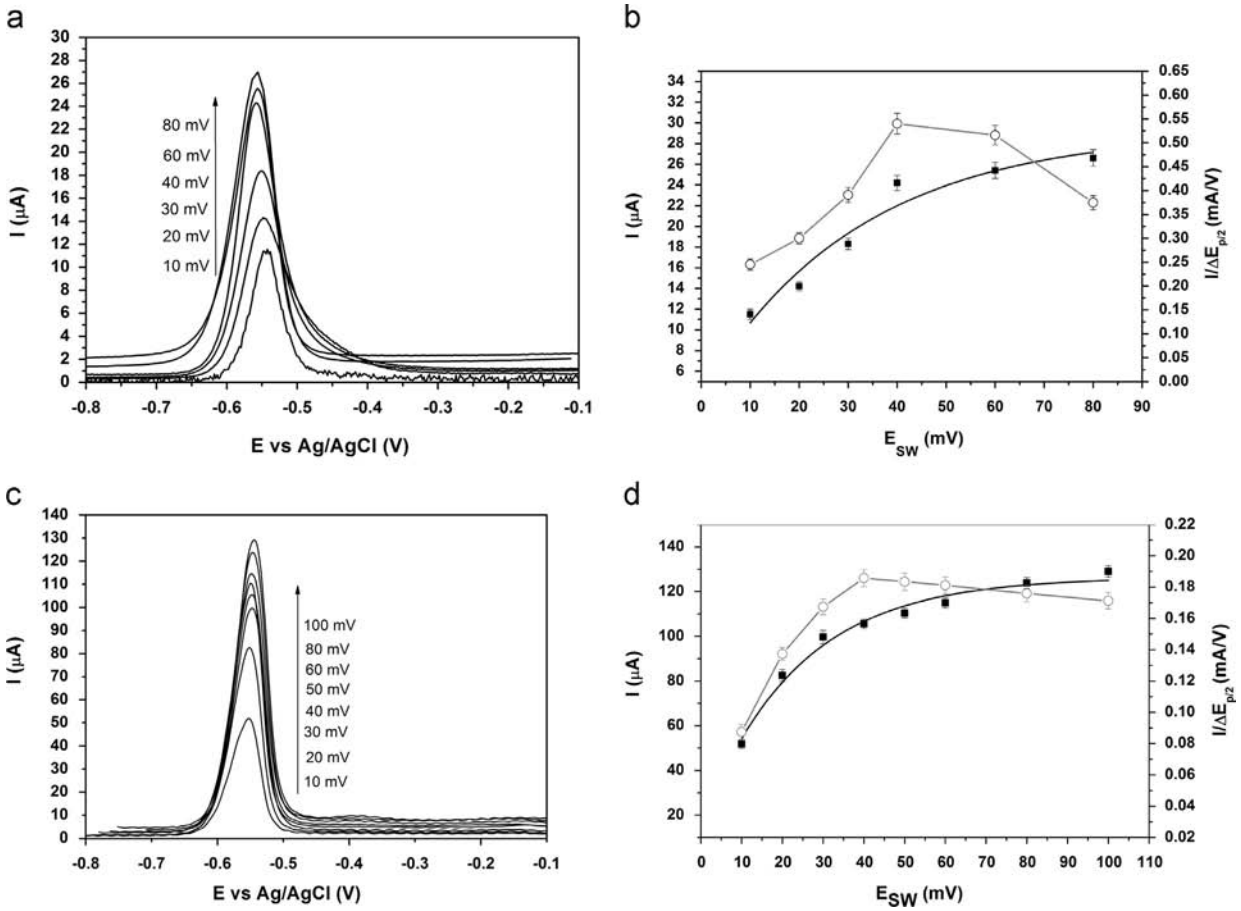

Fig. 6. The dependence of the net peak current (I) and net peak current /peak current width at half-height ratio ($I/\Delta E_{p/2}$) for (a) and (b) BDD 20,000 and (c) and (d) BDND 2000 with the square wave amplitude for experiments carried out under the following conditions: 100 μg/L Pb^{2+} in a ammonium acetate buffer (0.2 mol L^{-1}), deposition time = 180 s, ΔE_s = 2 mV and ν = 150 Hz.

Table 1
Dependence of the peak current width at half-height ratio as a function of the step potential increase.

Sample	$\Delta E_{p/2}$ (mV) ΔE_s (mV)				
	2	**4**	**6**	**8**	**10**
BDD 2000	75	78	79	83	89
BDD 20,000	94	95	96	99	98
BDND 2000	59	70	75	79	80
BDND 20,000	68	75	82	93	95

three to five times lower. The minimum concentration of each metal ion detectable with BDD was 50 μg L^{-1} Zn^{2+}, 1.0 μg L^{-1} Cd^{2+} and 5.0 μg L^{-1} Pb^{2+}. The authors also observed BDD exhibited an electrode-to-electrode and run-to-run variability of less than 5%, which is comparable to that for Hg-GC. Comparing the work of these authors with our was observed that was obtained higher sensitivity and lower detection limit (< 1 μg L^{-1}) with them, this results can be explained with better sensitivity and reduced background noise of the SWV compared to those of other voltammetric techniques such as ASV used for these authors.

Another important analytical parameter to compare is the linear dynamic range, which is taken from the response curves. The response curves exhibited a linear behavior for all the metal ions in both electrodes ranging from low to high 100 μg L^{-1} level with linear regression correlation coefficients of 0.99 or greater. Some studies have shown that BDD provides a linear dynamic range four times higher for various metal ions [2,7,25]. This range is comparable with those of mercury electrodes and it is more adequate in most analytical applications. Finally, BDD and BDND must be able to provide the same reproducible results as an Hg-based electrode. For all films tested, BDD and BDND showed a run-to-run variability of less than 5% R.S.D. (N = 3) and it is comparable to values for Hg-GC [7,49]. The reproducibility of the electrode was excellent with a variability of 3.8% for the BDD and 2.8% for the BDND both 20,000 mg L^{-1}, and the best result is shown in the nanocrystalline film with 2000 mg L^{-1}.

4. Conclusions

SWV parameter optimizations for lead detection using BDD and BDND films with two different doping levels were studied. The optimization study shows that lead system is reversible for all electrodes, micro and nanocrystalline films, and independent from doping level or grain size. However, the sensitivity of BDD films of 2000 ppm was significantly low, making the material useless for application in the detection of low levels of lead concentration. The results described above demonstrate that anodic stripping voltammetry in the BDD and BDND electrodes is a suitable mercury-free method for the determination of trace levels of lead in drinking water. Due to the unique electrochemical features of the polycrystalline diamond, a linear dependence between the stripping peak current and the lead concentration was found below 10 μg L^{-1}. The low detection limit, around 1 μg L^{-1}, which was shown in diamond films using the SWASV technique is similar

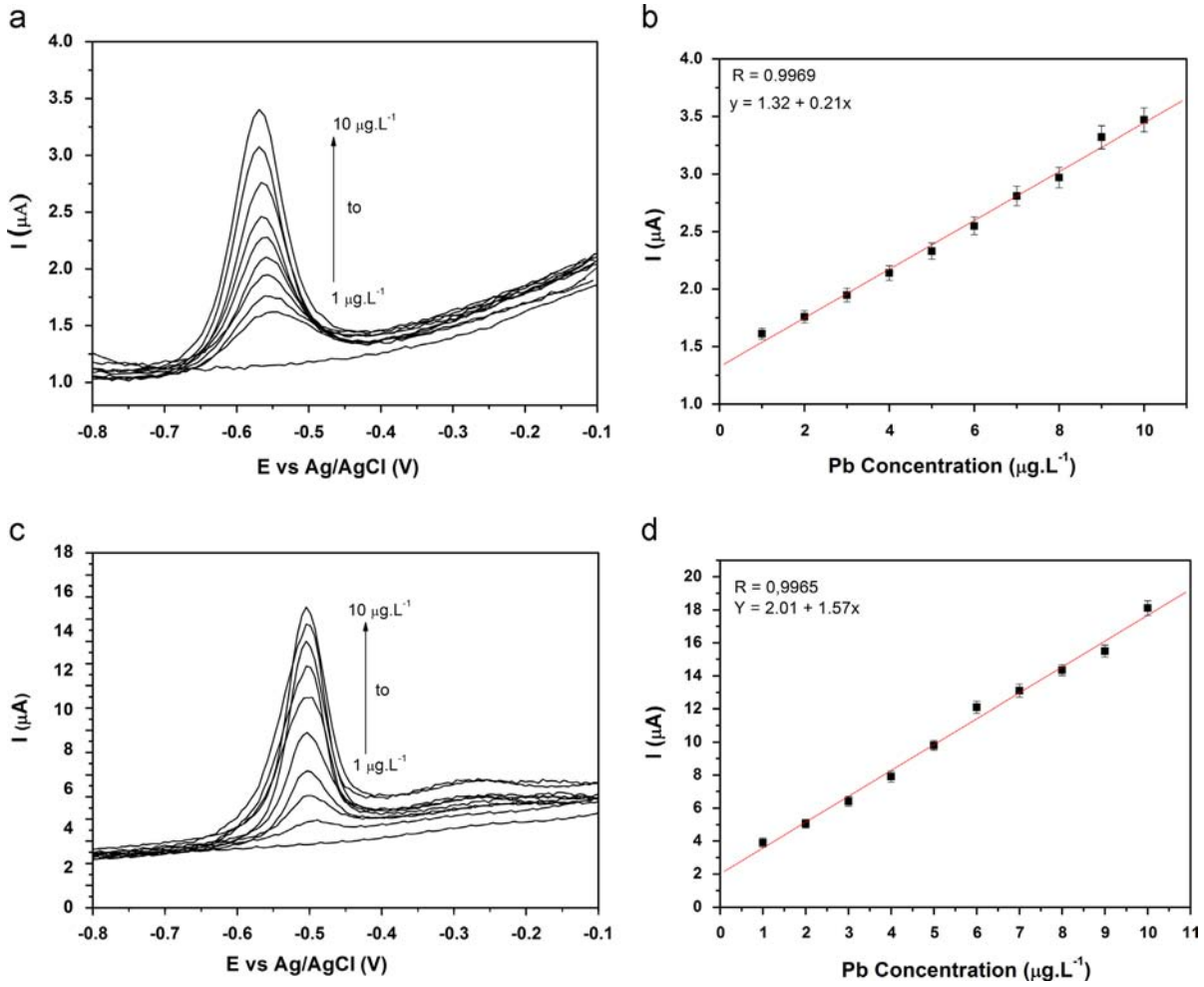

Fig. 7. SWASV curves for the stripping of Pb from solutions containing $Pb(NO_3)_2$ in 0.2 mol L^{-1} acetate buffer; deposition time = 180 s, E_{sw} = 40 mV, ΔE_s = 2 mV and ν = 150 Hz.

Table 2
Detection figures of merit for metal ions measured using BDD and BDND electrodes.

Parameter	Pb^{2+}		
	BDD 20,000	BDND 2000	BDND 20,000
Linear regression correlation	0.9969	0.9965	0.9964
Sensitivity (μA μg L^{-1})	0.21	1.57	1.07
DL (μg L^{-1})	0.98	0.57	0.77
QL (μg L^{-1})	3.20	1.70	2.65
Reproducibility (R.S.D. at 5 ppb n = 3) (%)	3.5	2.0	2.8

compared to mercury electrodes. Furthermore, the results were in excellent agreement with those reported for lead detection using HMDE polarography, demonstrating that diamond electrodes are a suitable mercury-free method to determine lead trace levels in water.

Acknowledgments

This work is supported by Brazilian National Institute of Science and Technology (INCT) for Climate Change funded by CNPq Grant number 573797/2008-0 e FAPESP Grant numbers 2008/57719-9 and 2012/00393-0.

References

[1] L. Järup, Br. Med. Bull. 68 (2003) 167–182.
[2] A. Manivannan, R. Kawasaki, D.A. Tryk, A. Fujishima, Electrochim. Acta 49 (2004) 3313–3318.
[3] T.M. Florence, J. Electroanal. Chem. Interfacial Electrochem. 27 (1970) 273–281.
[4] G.S. Reeder, W.R. Heineman, Sens. Actuators B 52 (1998) 58–64.
[5] A. Salimi, V. Alizadeh, R. Hallaj, Talanta 68 (2006) 1610–1616.
[6] P.R.M. Silva, M.A. ElKhakani, L. Gastonguay, R. Lacasse, M. Ladouceur, Anal. Chim. Acta 385 (1999) 249–255.
[7] E.A. McGaw, G.M. Swain, Anal. Chim. Acta 575 (2006) 180–189.
[8] Z. Chomistekova, J. Sochr, J. Svitkova, L. Svorc, Acta Chim. Slovaca 4 (2011) 11–17.
[9] O.E. Tall, N. Jaffrezic-Renault, M. Sigaud, O. Vittori, Electroanalysis 19 (2007) 1152–1159.
[10] V. Pedrosa, L. Codognoto, S. Machado, L. Avaca, J. Electroanal. Chem. 573 (2004) 11–18.
[11] T.L. Read, E. Bitziou, M.B. Joseph, J.V. Macpherson, Anal. Chem. 86 (2014) 367–371.
[12] E.C. Almeida, A.F. Azevedo, M.R. Baldan, J.M. Rosolen, N.G. Ferreira, Chem. Phys. Lett. 438 (2007) 47–52.
[13] N.G. Ferreira, E. Abramof, E.J. Corat, N.F. Leite, V.J. Trava-Airoldi, Diam. Relat. Mater. 10 (2001) 750–754.
[14] S. Wang, V.M. Swope, J.E. Butler, T. Feygelson, G.M. Swain, Diam. Relat. Mater. 18 (2009) 669–677.
[15] Y. Zhou, J. Zhi, X. Zhang, M. Xu, Diam. Relat. Mater. 20 (2011) 18–22.
[16] A.F. Azevedo, F.A. Souza, P. Hammer, M.R. Baldan, N.G. Ferreira, J. Nanopart. Res. 13 (2011) 6133–6139.
[17] A.F. Azevedo, N.A. Braga, F.A. Souza, J.T. Matsushima, M.R. Baldan, N.G. Ferreira, Diam. Relat. Mater. 19 (2010) 462–465.
[18] A.E. Fisher, Y. Show, G.M. Swain, Anal. Chem. 76 (2004) 2553–2560.
[19] P.W. May, W.J. Ludlow, P.J. Heard, J.A. Smith, K.N. Rosser, Diam. Relat. Mater. 17 (2008) 105–117.

[20] P. Sonthalia, E. McGaw, Y. Show, G.M. Swain, Anal. Chim. Acta 522 (2004) 35–44.
[21] G.G. Honório, G.C. Azevedo, M.A.C. Matos, M.A.L. Oliveira, R.C. Matos, Food Control 36 (2014) 42–48.
[22] S.K. Lovric, B. Nigovic, J. Electroanal. Chem. 593 (2006) 125–130.
[23] M. Lovric, S.K. Lovric, J. Electroanal. Chem. 248 (1988) 239–253.
[24] D. Souza, S.A.S. Machado, L.A. Avaca, Quim. Nova 26 (2003) 81–89.
[25] L. Codognoto, S.A.S. Machado, L.A. Avaca, Diam. Relat. Mater. 11 (2002) 1670–1675.
[26] D. Souza, L. Codognoto, A.R. Malagutti, R.A. Toledo, V.A. Pedrosa, R.T.S. Oliveira, L.H. Mazo, L.A. Avaca, S.A.S. Machado, Quim. Nova 27 (2004) 790–797.
[27] T.M.B.F. Oliveira, H. Becker, E. Longhinotti, D. Souza, P. Lima-Neto, A.N. Correia, Microchem. J. 109 (2013) 84–92.
[28] R. Inam, C. Bilgin, J. Appl. Electrochem. 43 (2013) 425–432.
[29] M. Lovric, D. Jadresko, S.K. Lovric, Electrochim. Acta 90 (2013) 226–231.
[30] R. Issaoui, J. Achard, F. Silva, A. Tallaire, V. Mille, A. Gicquel, Phys. Status Solidi A 208 (2011) 2023–2027.
[31] A.F. Azevedo, S.C. Ramos, M.R. Baldan, N.G. Ferreira, Diam. Relat. Mater. 17 (2008) 1137–1142.
[32] A.N. Jones, W. Ahmed, I.U. Hassan, C.A. Rego, H. Sein, M. Amar, M.J. Jackson, J. Phys.: Condens. Matter 15 (2003) S2969–S2975.
[33] V. Baranauskas, H.J. Ceragioli, A.C. Peterlevitz, M.C. Tosin, S.F. Durrant, Thin Solid Films 377 (2000) 303–308.
[34] M. Bernard, C. Baron, A. Deneuville, Diam. Relat. Mater. 13 (2004) 896–899.
[35] F. Piazza, A. Golanski, S. Schulze, G. Relihan, Appl. Phys. Lett. 82 (2003) 358–360.
[36] A.C. Ferrari, J. Robertson, Phys. Rev. B: Condens. Matter 63 (2001) 14095–14107.
[37] M. Bernard, A. Deneuville, P. Muret, Diam. Relat. Mater. 13 (2004) 282–286.
[38] J.P. Goss, P.R. Briddon, Phys. Rev. B: Condens. Matter 73 (2006) (085203-1–085204-8).
[39] A.C. Ferrari, J. Robertson, Philos. Trans. R. Soc. Lond. A 362 (2004) 2269–2270.
[40] F. Silva, F. Bénédic, P. Bruno, A. Gicquel, Diam. Relat. Mater. 14 (2005) 398–403.
[41] Y.V. Pleskov, Russ. J. Electrochem. 38 (2002) 1275–1291.
[42] J.G. Osteryoung, R.A. Osteryoung, Anal. Chem. 57 (1985) 101–110.
[43] M. Lovric, Square-wave Voltammetry. Theory and Application, Springer, New York, 2002.
[44] M. Lovric, M. Branica, J. Electroanal. Chem. 226 (1987) 239–251.
[45] J.J. O'Dea, J.G. Osteryoung, R.A. Osteryoung, Anal. Chem. 53 (1981) 695–701.
[46] K.H. Wong, R.A. Osteryoung, Electrochim. Acta 32 (1987) 629–631.
[47] M. Lovric, S.K. Lovric, Int. J. Electrochem. (2012) 1–7.
[48] R.F. Teófilo, H.J. Ceragioli, A.C. Peterlevitz, L.M. Da Silva, F.S. Damos, M.M. C. Ferreira, V. Baranauskas, L.T. Kubota, J. Solid State Electrochem. 11 (2007) 1449–1457.
[49] M.C. Granger, M. Witek, J.S. Xu, J. Wang, M. Hupert, A. Hanks, M.D. Koppang, J.E. Butler, G. Lucazeau, M. Mermoux, J.W. Strojek, G.M. Swain, Anal. Chem. 72 (2000) 3793–3804.
[50] M. Hupert, A. Muck, R. Wang, J. Stotter, Z. Cvackova, S. Haymond, Y. Show, G.M. Swain, Diam. Relat. Mater. 12 (2003) 1940–1949.
[51] P.H. Chen, M.A. Fryling, R.L. McCreery, Anal. Chem. 67 (1995) 3115–3122.
[52] D. Dragoe, N. Spataru, R. Kawasaki, A. Manivannan, T. Spataru, D.A. Tryk, A. Fujishima, Electrochim. Acta 51 (2006) 2437–2441.